

Assessment of the relation between ion beam mixing, electron–phonon coupling and damage production in Fe

C. Björkas *, K. Nordlund

Department of Physics, University of Helsinki, P.O. Box 43, FI-00014 Helsinki, Finland

ARTICLE INFO

Article history:

Received 10 February 2009

Received in revised form 4 March 2009

Available online 17 March 2009

PACS:

61.72.–J

61.80.Hg

63.20.Kd

64.75.Ef

34.20.Cf

Keywords:

Fe

Ion beam mixing

Electron–phonon coupling

Displacement cascades

Interatomic potentials

ABSTRACT

As a step in the process of assessing the reliability of interatomic potentials for iron, we compare experimental measurements of ion beam mixing with values obtained from molecular dynamics simulations. We include the electron–phonon coupling (EPC) model by Hou et al. [Q. Hou, M. Hou, L. Bardotti, B. Prével, P. Mélinon, A. Perez, Phys. Rev. B 62 (2000) 2825] in the simulations and consider a range of coupling strengths. Three different iron interatomic potentials are used. We discuss the effect of the coupling on the primary damage and how the damage is influenced by different velocity minima for applying electron stopping.

© 2009 Elsevier B.V. All rights reserved.

1. Introduction

The reliability of iron interatomic potentials is not yet established, since the description of primary damage often varies from one potential to another. Although the variation when comparing all potentials is very large [2], we have recently shown that when only the modern potentials that describe the energetics of interstitials reasonably are included in the comparison, the discrepancy is much smaller [3]. In that study, however, the uncertainty in how the transfer of energy from the atomic to the electronic subsystem (electronic stopping S_e [4] and electron–phonon coupling (EPC) [5]) should be treated was not considered. Unfortunately there are large uncertainties in how these should be treated at low (of the order of 1–10 eV) atom kinetic energies [6–8]. To reduce the uncertainties in the damage production, S_e , and EPC, one could benefit from comparisons to experimental quantities that directly depend on the cascade development. One of these quantities is the ion beam mixing (IBM).

IBM is simply the athermal relocation of atoms from their lattice sites by ion irradiation. This mixing is experimentally measur-

able by for instance observing the broadening of a marker layer under ion irradiation [9]. In iron, only two of these experiments have been done, yielding mixing efficiencies of 4.5–4.6 Å⁵/eV [9] and 7.2, 8.1 Å⁵/eV [10,11], respectively.

The mixing crucially depends on the cascade development, since ion irradiation produces multiple cascades. In these, the energy end heat distributions are consequential, implying that correct descriptions of electronic stopping S_e and electron–phonon coupling (EPC) are required. S_e slows down ballistic atoms and thus reduces the cascade region and with that also the mixing. However, uncertainties regarding this quantity exist, e.g. the lowest energy at which the electronic friction should be applied is debated [7]. EPC also reduces the mixing, since a coupling between the electrons and the lattice results in a fast distribution of the heat from the hot cascade core to the cooler electronic gas. This suppresses the liquid region in which the atoms can redistribute and mix. In metals, the thermal conductivity is handled predominantly by the electrons in the beginning of a cascade [5,12], which indicates that the EPC could play an important role in iron.

When modelling cascades with molecular dynamics (MD) simulations methods, the EPC is not taken into account in the conventional MD algorithms [13], but can be added with various schemes [1,14–19]. Studies of the effect of EPC on cascade damage in a

* Corresponding author. Tel.: +358 9 1915 0003; fax: +358 9 1915 0042.
E-mail address: carolina.bjorkas@helsinki.fi (C. Björkas).

range of coupling strengths in Fe have been done [16,20,21] with the conclusion that a strong coupling has an influence on the resulting damage. However, the actual coupling strength in iron has not been determined, hence, the importance of including EPC models in cascade simulation in iron is still unclear.

Here we carry out a systematic study of the role of the EPC and S_e in iron cascades by reproducing an IBM experiment with molecular dynamics methods. We use three different iron potentials and we assess how the quantities affect the primary damage.

2. Methods

2.1. Simulating the ion beam mixing

The Kim et al. iron IBM experiment [9] was done at 6 K with 650 keV Kr ions irradiating Fe, with Pt and Au used as tracer. Pt tracers were also used in the other experiment [10], where iron matrices were irradiated by 150 keV Ar ions. Temperatures in the range 18–345 K were used, resulting in two different values (a lower for 20 K and a higher for 29–345 K). The large amount of oxygen impurities in this experiment resulted in large uncertainties, hence, the Kr experiment can be considered more accurate and therefore we chose to simulate that one.

The IBM simulations were done in two steps. First, molecular dynamics (MD) range calculations were performed to obtain the recoil spectrum $n(E)dE$ of the Kr ions irradiating Fe. The spectrum and the deposited nuclear energy was calculated in the range 200–600 Å from the surface, and the marker layers in the corresponding experiment were deposited at a depth of 400 Å. (The thickness of the markers in the experiment was 5–15 Å.) The angle between the beam and the normal to the surface was $\theta = 10^\circ$ in both the experiments and the simulations and ϕ was additionally varied randomly in the 0–360° interval in the simulations.

Full MD simulations (at 300 K) were used to simulate cascades caused by self-recoils, the energies of which ranged from 0.5 to 200 keV. At least 10 cases for each energy were simulated, the exception being the 200 keV recoils, of which only 6 events were simulated. Three different Fe potentials were used: AMS [22], DD-BN [23,3] and MEA-BN [24,3].

From the cascades, the square of the total atom displacement, R^2 , was obtained. This corresponds to the difference between the positions of the atoms at the end and the beginning of a cascade, i.e.

$$R^2 = \sum_i (r_i(t) - r_i(t=0))^2. \quad (1)$$

A function was fitted to the data points in order to be able to inter- and extrapolate. The function takes both the low and high (sub-cascade formation) energy dependency into account.

$$R^2(E) = \frac{aE^{3/2}}{b^{1/2} + E^{1/2}} \quad (2)$$

The experimentally measured normalized mixing efficiency is defined as

$$Q_{exp} = \frac{Dt}{\Phi F_{D_n}}, \quad (3)$$

where D is an effective diffusion coefficient for mixing, t is the implantation time, Φ the ion fluence and F_{D_n} the deposited nuclear energy per unit depth [9]. The unit of the efficiency is $\text{Å}^5/\text{eV}$. Using the atomic definition of the diffusion coefficient, $D = \frac{\langle r^2 \rangle}{6t}$, this is equal to the simulated mixing

$$Q_{sim} = \frac{R^2}{6n_0 E_{D_n}}, \quad (4)$$

where n_0 is the atomic density (in a BCC material, the atomic density is $n_0 = 2/a_0^3 \cdot a_0^{\text{DD-BN}} = 2.86 \text{ Å}$, $a_0^{\text{MEA-BN}} = 2.89 \text{ Å}$ and $a_0^{\text{AMS}} = 2.86 \text{ Å}$ at 300 K). E_{D_n} is the deposited nuclear energy.

The total cumulative mixing efficiency resulting from the ion irradiation is obtained by

$$Q_{sim}^{tot}(E_0) = \frac{\int_0^{E_0} R^2(E)n(E)dE}{6n_0 E_{D_n}}, \quad (5)$$

where E_0 is the ion energy (650 keV for Kr, 150 keV for Ar) and $n(E)dE$ is the above mentioned primary recoil spectrum. This method for relating simulated and experimental values of the mixing efficiency has previously been employed successfully for different materials [25].

2.2. The electron–phonon coupling

The EPC coupling model of Hou [1] was implemented into the cascade simulations. Details of the model is found in [1,5,12] and is here only described briefly. The electronic system is considered as a heat bath of temperature T_e , and when ignoring the phonon diffusion, the change in the temperature of the ionic system is expressed as

$$\frac{dT_i(t)}{dt} = -\alpha(T_i(t) - T_e), \quad (6)$$

where (using the Sommerfeld free electron theory)

$$\alpha = \frac{\Theta_D L n e^2 k_B Z T_e}{2 m_e \kappa \epsilon_F}. \quad (7)$$

Θ_D is the Debye temperature, L = Lorentz number, n = electron density, e = the electron charge, k_B = Boltzmann's constant, Z is the valence, m_e = the electron mass, κ = thermal conductivity and ϵ_F = the Fermi energy. The values for these parameters in iron are found in Table 1. The time constant for the coupling is $\tau = \alpha^{-1}$ and a large time constant indicates a strong coupling.

The electron–phonon energy exchange can be described as a damping force. This force, acting on atom i with the velocity \mathbf{v}_i , can be written as

$$\mathbf{F}_i = -\mu \mathbf{v}_i, \quad (8)$$

where

$$\mu = m_i \alpha \frac{T_i - T_e}{T_i}. \quad (9)$$

In order to avoid singularities as the velocities are approaching zero, this expression is written as

$$\mu = m_i \alpha \frac{T_i - T_e}{[T_i^2 + (T_e/20)^2]^{1/2}}. \quad (10)$$

The factor 1/20 was chosen to be compatible with the time steps used in MD [12].

This damping is included in the MD code together with the electronic stopping which also acts as a damping force. The two forces have to be joined at some suitable velocity. The electronic stopping dominates at high velocities and should not be applied to low-energy ions (otherwise the linear dependence on velocity quenches any simulations down to 0 K). Therefore, below a velocity corresponding to the cohesive energy of iron, only damping due to

Table 1
Constants used in the calculation of the EPC time constant of iron [26,27].

Θ_D	420 K
L	2.61 W ohm/K ²
n	$17.0 \cdot 10^{28} \text{ m}^{-3}$
Z	2
κ	0.8 W/(cm K)
ϵ_F	11.1 eV
m_{Fe}	55.85u

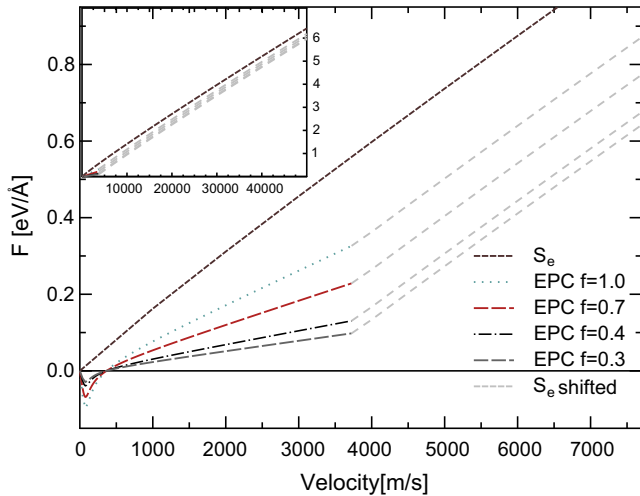


Fig. 1. The electron–phonon coupling (EPC) at 300 K for Fe and Au as a function of ion velocity. The electronic stopping S_e is also included and it is scaled so as to join the EPC at a velocity corresponding to the cohesive energy.

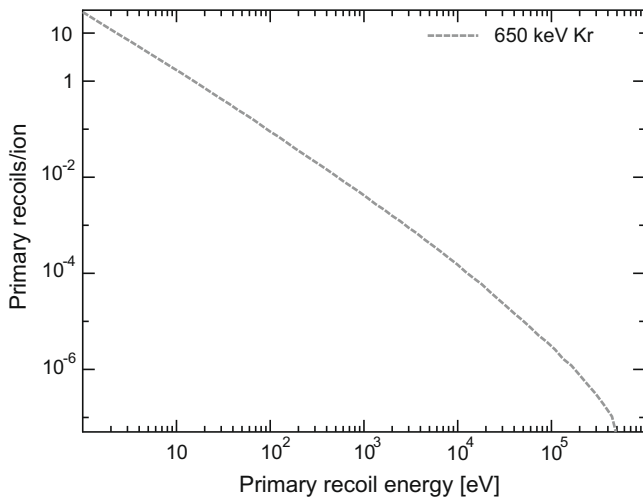


Fig. 2. The primary recoil spectrum in the depth 200–600 Å obtained for 650 keV Kr ions bombarding Fe.

EPC is considered. A join without any splining function is constructed by scaling the electronic stopping so that the S_e and EPC coincide at $v = \sqrt{2E_{coh}/m_i} = 3724$ m/s. This meant that a constant of 0.132 eV/Å was subtracted from the ZBL electronic stopping [4] (see Fig. 1). The electronic stopping could be proportional to v or to $(v - v_0)$, hence, the small scaling is justified. This is illustrated in Fig. 1 and the scaling is seen to be negligible at high velocities.

The calculated time constant for iron at $T_e = 300$ K is $\tau_{Fe} = 0.654102$ ps, which means that the EPC is much stronger in iron when compared to, e.g. Au ($\tau_{Au} = 20.5241$ ps), the reason being the higher electron conductivity in Au.

In this method, the electron temperature is considered to be constant during the simulations, which effectively means that the electronic thermal diffusivity is infinite. However, Rutherford and Duffy [21] employed a method in which the temperature of the electron thermostat was allowed to vary, showing a significant increase in temperature at the very beginning of a cascade. Electron temperature variation will affect the defect evolution (to an unknown extent), but it is nevertheless not included in our simulations.

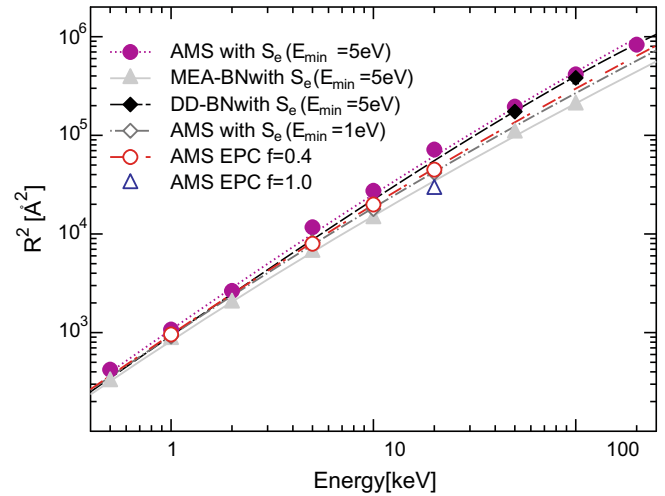


Fig. 3. The atom displacement R^2 as a function of cascade energy. Data for the three different potentials are shown and also AMS results using different minima values for the electronic stopping S_e and different electron–phonon coupling (EPC) strengths.

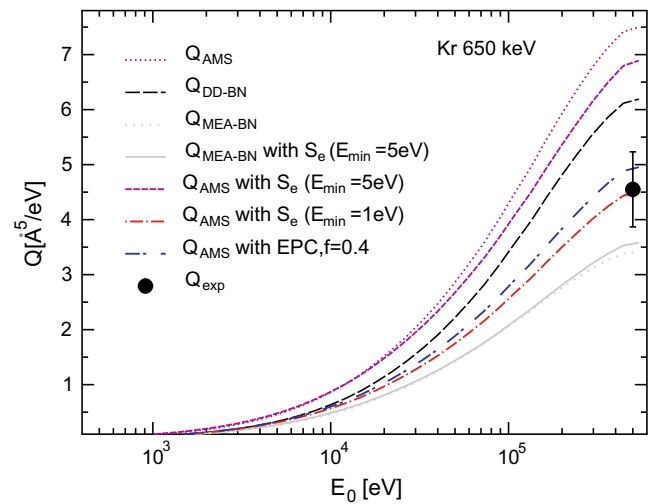


Fig. 4. The cumulative simulated mixing efficiency $Q_{sim}^{tot}(E_0)$ as a function of primary recoil energy. The endpoint on the right side corresponds to the experimental irradiation. Data are shown for three different iron potentials with the electronic stopping correction (see Appendix). Data for the AMS and MEA-BN with included electronic stopping S_e during the cascades are also shown. In addition to this, AMS results with $S_e(E_{min} = 1$ eV) and with a scaled electron–phonon coupling (EPC) strength are shown. The experimental value is taken from [9].

3. Results and discussion

3.1. Without the EPC

The obtained recoil spectra for the two different ion beams are seen in Fig. 2. The calculated total nuclear deposited energy in the depth 200–600 Å for the Kr beam is 123.448 keV (308.6 eV/Å).

We also considered the possibility of applying electronic stopping to ions with velocities ≥ 1 eV instead of ≥ 5 eV. This test was performed with the AMS potential in 1, 5, 10 and 20 keV cascades.

In Fig. 3, values of the $\langle R^2 \rangle$ -displacements are shown. For the DD-BN values, the electronic stopping corrections (see Appendix) were done and for the MEA-BN only results with $S_e(E_{min} = 5$ eV) are shown. Data for AMS with both $S_e(E_{min} = 5$ eV) and $S_e(E_{min} = 1$ eV) are included.

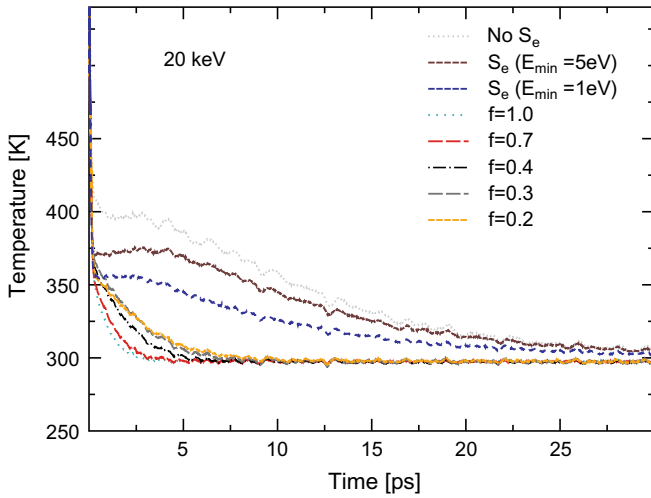


Fig. 5. The temperature during a 20 keV cascade with different EPC strengths and with different S_e criteria. In the case “No S_e ”, no electron stopping nor EPC is used.

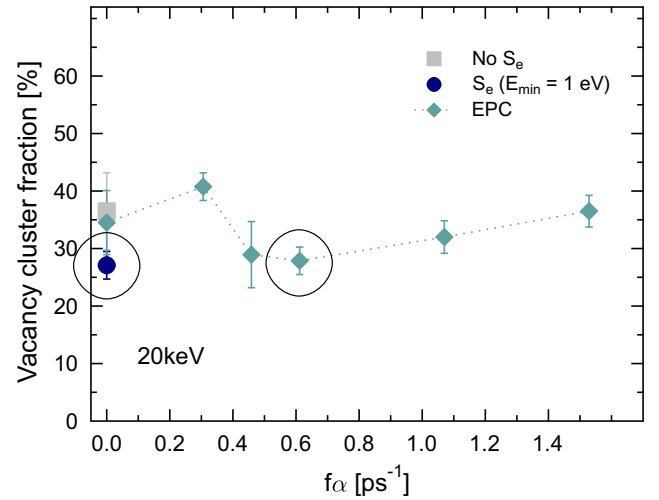


Fig. 7. The fraction of vacancies in clusters after 20 keV cascades with different EPC strengths and with different S_e criteria. In the case $f\alpha = 0$, no EPC is used and E_{min} in the S_e is 5 eV. The points corresponding to the conditions that lead to a correct mixing are encircled.

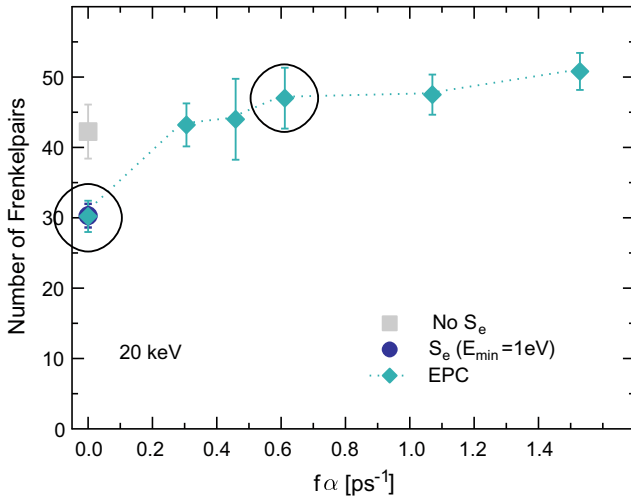


Fig. 6. The number of Frenkel pairs after 20 keV cascades with different EPC strengths and with different S_e criteria. In the case $f\alpha = 0$, no EPC is used and E_{min} in the S_e is 5 eV. The points corresponding to the conditions that lead to a correct mixing are encircled (i.e. $S_e(E_{min} = 1 \text{ eV})$ and $f = 0.4$).

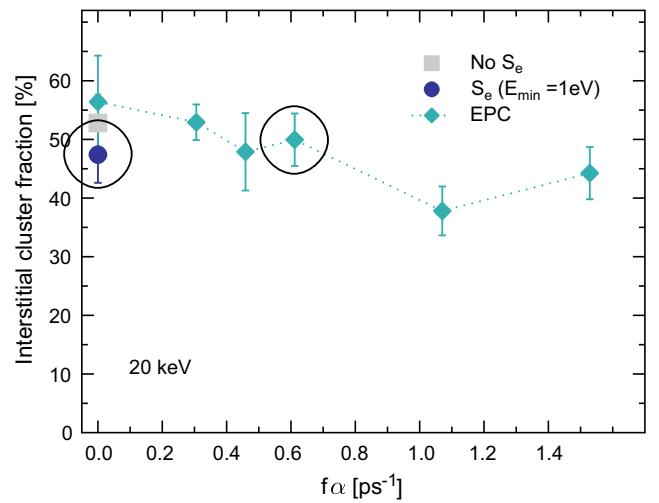


Fig. 8. The fraction of interstitials in clusters after 20 keV cascades with different EPC strengths and with different S_e criteria. In the case $f\alpha = 0$, no EPC is used and E_{min} in the S_e is 5 eV. The points corresponding to the conditions that lead to a correct mixing are encircled.

The cumulative simulated mixing efficiency, $Q_{sim}^{tot}(E_0)$ Eq. (5), was calculated and the results are illustrated in Fig. 4. As the figure shows, the potentials result in three different mixing values for each ion bombardment (considering only the $S_e(E_{min} = 5 \text{ eV})$ cases). The AMS yields the highest value ($6.9 \pm 0.1 \text{ \AA}^5/\text{eV}$ (Kr)) and the MEA-BN the lowest ($3.7 \pm 0.3 \text{ \AA}^5/\text{eV}$ (Kr)). The DD-BN lies in the middle with a mixing efficiency of $6.2 \pm 0.3 \text{ \AA}^5/\text{eV}$ (Kr). The errors come from the uncertainties in the calculations of the R^2 -values.

In order to relate the simulated values to the experimental one, the experimental uncertainties (arising mostly from impurities in the samples) must be included. These are approximated to about 15% for the Kr experiments, resulting in an efficiency in the range $3.8\text{--}5.2 \text{ \AA}^5/\text{eV}$.

The results of the MEA-BN potential are below the experimental value and the values of DD-BN and AMS are slightly above. The likely reason for the differences between the potentials can be found in the description of the melting temperatures of each potential: $T_{melt}^{MEA-BN} = 2300 \pm 25 \text{ K}$, $T_{melt}^{DD-BN} = 2125 \pm 25 \text{ K}$ and $T_{melt}^{AMS} =$

$1750 \pm 25 \text{ K}$ [3]. The experimental temperature is $T_{melt}^{exp} = 1811 \text{ K}$ [28]. The order here is now the opposite (higher melting T , lower mixing efficiency). Hence, there is a correlation between the melting temperature and the mixing in iron. This correlation has been observed in other materials as well [29] and it derives from the fact that a lower melting point results in a larger melted cascade core in which the atoms easily mix. Correspondingly, a high melting temperature means a small melted region, yielding a small mixing efficiency.

Using $S_e(E_{min} = 1 \text{ eV})$ and the AMS potential we arrive at a mixing value of $4.5 \pm 0.1 \text{ \AA}^5/\text{eV}$, which is in perfect agreement with the experiments.

3.2. Including the EPC

Five 20 keV cascades with S_e and EPC as described above were simulated with the AMS. A comparison of these with 20 keV cascades where no EPC was used showed that this EPC model has a

Table 2

The ion beam mixing in the AMS potential with electron–phonon coupling (EPC) of different strengths and with different velocity minima in the application of electronic stopping S_e . τ' is the time constant (the inverse of α , Eq. (7)) scaled with an arbitrary parameter $1/f$. R^2 is Eq. (1) for 20 keV cascades and Q' is $Q_0 \cdot R^2/R_0^2$, where the sub-index refers to values obtained without any EPC and with $S_e(E_{min} = 5 \text{ eV})$. In the whole spectrum calculations R^2 values from 1 to 20 keV cascades were used (except for the $S_e(E_{min} = 5 \text{ eV})$ simulations where the cascade energies were in the 0.5–200 keV range). The experimental value is from [9].

	τ' (ps)	R^2 (\AA^2)	Q' ($\text{\AA}^5/\text{eV}$)
$S_e(E_{min} = 5 \text{ eV})$	–	71770 ± 2900	6.9 ± 0.1
$S_e(E_{min} = 1 \text{ eV})$	–	43340 ± 1490	4.2 ± 0.3
$f = 1.0$	0.6541	28530 ± 1270	2.7 ± 0.3
$f = 0.7$	0.9344	34840 ± 2830	3.3 ± 0.4
$f = 0.4$	1.6352	44910 ± 4420	4.3 ± 0.5
$f = 0.3$	2.1803	49810 ± 1780	4.8 ± 0.4
$f = 0.2$	3.2705	58390 ± 2620	5.6 ± 0.5
Whole spectrum	τ' (ps)		Q ($\text{\AA}^5/\text{eV}$)
$S_e(E_{min} = 5 \text{ eV})$	–		6.9 ± 0.1
$S_e(E_{min} = 1 \text{ eV})$	–		4.5 ± 0.1
$f = 0.4$	1.6352		5.0 ± 0.2
Exp.			$3.8\text{--}5.2$ (6 K)

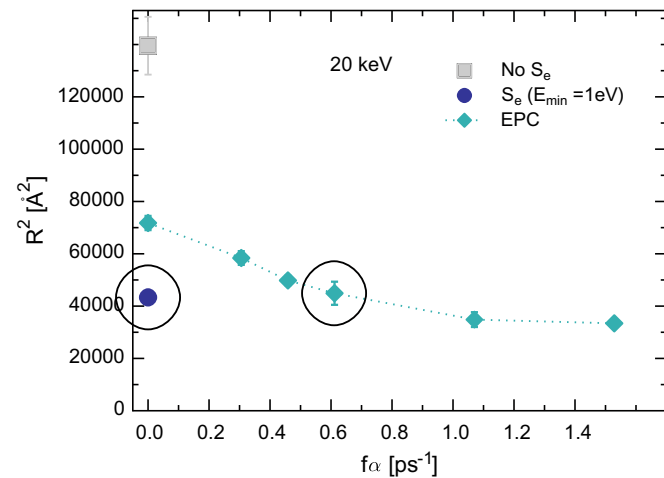


Fig. 9. The square of the total atom displacement R^2 in 20 keV cascades with different EPC strengths and with different S_e criteria. Note that in the case $f\alpha = 0$, no EPC is used and E_{min} in the S_e is 5 eV. The points corresponding to the conditions that lead to a correct mixing are encircled.

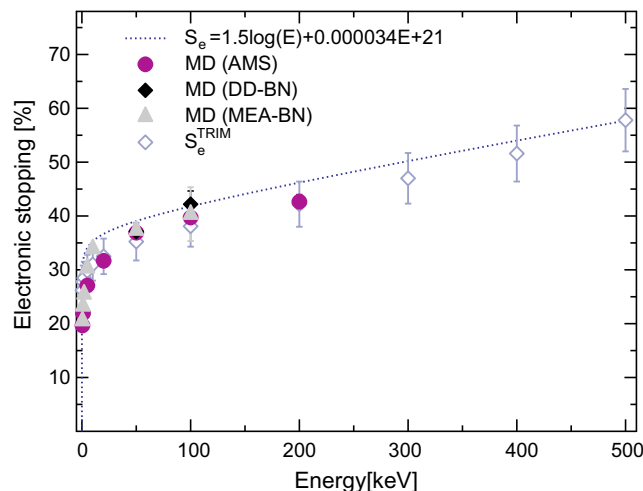


Fig. 10. The electronic stopping (expressed as percentage of the recoil energy) as a function of recoil energy. Data are shown for both TRIM and MD calculations.

large effect. The R^2 -values are namely reduced with about 60%, the number of Frenkel pairs goes from 30 ± 3 to 51 ± 3 , the vacancy clustered fraction from $34 \pm 6\%$ to $36 \pm 6\%$ and the interstitial clustered fraction goes from $56 \pm 4\%$ to $44 \pm 5\%$ (see Figs. 6–8). Assuming that the mixing parameter Q scales linearly with the R^2 -values, we end up with a Q -value of $2.7 \pm 0.3 \text{ \AA}^5/\text{eV}$ (see Table 2), which is too low. A downscaling of the EPC strength is therefore done, in order to obtain $Q \approx 4.6 \text{ \AA}^5/\text{eV}$.

The scaling was done by simply multiplying a “fitting parameter” f with the inverse of the time constant α Eq. (7), so that $1/\alpha' = 1/f\alpha = \tau'$. We used $f = 0.7, 0.4, 0.3$ and 0.2 , which resulted in time constants of $\tau' = 0.934432, 1.63526, 2.18034$ and 3.2705 ps, respectively. In all cases, a new ν_0 was found for the ZBL elstop scaling in order to join it with the EPC at $\nu = \sqrt{2E_{coh}/m_i}$, as earlier. After this, five 20 keV cascades were simulated with all values of f . Furthermore, 1, 5 and 10 keV cascades were simulated for $f = 0.4$.

Table 2 contains the resulting Q -values. Coupling strengths of 1.64–2.18 ps end up in the same value as the experiment. Results from cascades with no EPC and S_e for atoms with energies above 1 eV also agree with the experiments.

The effect of EPC on the temperature during 20 keV cascades can be seen in Fig. 5. A stronger coupling means a faster cooling to the electronic temperature (300 K). Note that in the case of no EPC, the outermost regions of the simulation cell were controlled to 300 K. In Fig. 9, the R^2 -values Eq. (1) are plotted as a function of coupling strength. The relation is almost linear and a strong coupling leads to small displacement values, consistent with our discussions above.

The differences in the damage after 20 keV cascades with different coupling strengths are illustrated in Figs. 6–8. Noteworthy is that the defect production is similar in the case where no EPC with $S_e(E_{min} = 1 \text{ eV})$ is used and for $f = 0.3 - 0.4$. The points corresponding to the conditions that reproduce a correct mixing are encircled in the figures.

The circles show that adding EPC with a coupling strength scaled to the mixing have, considering the statistical errors, little effect on the vacancy cluster fraction but result in an increase in the number of Frenkel pairs with about 50%. Since EPC shortens the lifetime of a thermal spike, this indicates that most of the surviving clusters must be created during the ballistic phase. Single defects, however, have less time to recombine during the heat spike with a strong coupling, which results in an increase in residual defects. Gao et al. saw that the cluster fractions were affected in 1, 5 and 10 keV cascades only when really strong coupling con-

stants ($> 8.5 \text{ ps}^{-1}$) were used [20]. The interstitial cluster fraction was seen to increase, which was believed to be due to quenched-in defects after the ballistic phase. The effect was larger in 10 keV cascades than in 5 keV cascades. Here, in 20 keV cascades, the behaviour is different, with a smaller fraction at stronger coupling. At coupling strengths above 1.6 ps the effect is, however, negligible when taking the statistical errors into account.

A different S_e criteria only affected the cascade outcome in terms of vacancy clusters and atomic displacements R^2 . In the former case, a slight decrease in vacancy cluster fraction is seen when $E_{min} = 1 \text{ eV}$ compared to $E_{min} = 5 \text{ eV}$. The reduction of R^2 is, however, as large as 40%, again highlighting the impact of temperature variations during the first pico-seconds of a cascade (see Fig. 5).

4. Conclusions

An EPC strength with which experimental IBM mixing efficiency in iron could be reproduced was determined and the effect of different S_e criteria on the process was studied. How the primary damage was affected by these two quantities was also analyzed. We found that including S_e for atoms with kinetic energies above 5 eV, the experimental value of the IBM efficiency can not be reproduced without taking the electron–phonon coupling into account in the simulations. If, however, the limit is 1 eV, the simulated mixing agrees well with the experimental one.

Using the Hou et al. EPC model as such in AMS simulations resulted in a reduction of the mixing efficiency that was too large. A downscaling of the coupling strength with factors of 0.3–0.4 resulted in better agreement.

To summarize the results on mixing, we found that the AMS potential using either a minimum in the electronic stopping of 1 eV, or an electron–phonon coupling with a time constant of about 1.6–2.2 ps gave ion beam mixing values that agree with experiments. We then compared the damage production obtained using these models to assess how the uncertainty in choice of electronic stopping and electron–phonon coupling is reflected in defect production. We found that there is no statistically significant difference in the fraction of clustered defects, but the production of Frenkel pairs differs by $\sim 50\%$.

Of the three potentials that were used one (MEA-BN) is unsuitable for mixing simulations due to its overestimation of the melting point, which results in a low mixing efficiency. Since the EPC will reduce the mixing, including it will only make the underestimation of the mixing larger.

In conclusion, the total amount of primary damage depends on the applications of S_e and strength of EPC in cascades. The defect cluster fractions are, however, not affected.

Acknowledgements

This work, supported by the European Communities under the contract of Association between EURATOM/Tekes, was carried out within the framework of the European Fusion Development Agreement and the EU FP7-GETMAT Project. The views and opinions expressed herein do not necessarily reflect those of the European Commission. Grants of computer time from CSC, the IT Centre for Science in Espoo, Finland, are gratefully acknowledged.

Appendix A. Determination of electronic stopping

Some of the current simulations were ran without electronic stopping, since the defect comparison in them was compared to other publications on damage in Fe [30,3] where electronic stopping also was not included. Such runs do not directly correspond to any experimental recoil energy, since experimentally induced

cascades of course always include electronic stopping. However, the recoil energy E_{rec} in such runs can be rescaled to correspond to experimental primary recoil energies E_{elstop} by adding the electronic energy deposition for a higher-energy recoil E_{elstop} such that make the nuclear energy deposition for this recoil energy matches E_{rec} . To this end, we examined in detail the total amount of electronic energy deposition.

Electronic stopping was applied in the whole recoil energy range for atoms with kinetic energies above 5 eV for the AMS and MEA-BN potentials, but only for 50 and 100 keV cascades in DD-BN cascades. At these two energies the stopping was, however, seen to be, within statistical errors, the same in all three potentials (see Fig. 10), so the stopping in DD-BN at lower energies can be approximated to be the same as in the other potentials.

The stopping was also simulated with TRIM [31] to get the behaviour at higher energies ($> 200 \text{ keV}$). The TRIM displacement threshold value was scaled so that the stopping would agree with the MD value at 5 keV. The amount of the electronic stopping (in percentage of the recoil energy) at different energies according to TRIM and MD are seen in Fig. 10. A function was fitted to MD data at low energies and to TRIM data at energies above 200 keV (10% uncertainties were added to the TRIM values). The function best describing the elstop behaviour was a logarithmic one

$$f_{elstop} = a \cdot \log(E_{rec}) + bE_{rec} + c, \quad (11)$$

where $a = 1.5$, $b = 3.4 \cdot 10^{-5}$ and $c = 21$. The $R^2(E)$ -function in Eq. (5), is a function of recoil energy with electronic stopping included, i.e. $R^2(E_{elstop})$. As stated above, the cascade energies in the DD-BN cases must be scaled in order to take this into account. In other words,

$$E_{elstop} = E_{rec}(1 - (a \cdot \log(E_{rec}) + bE_{rec} + c)/100), \quad (12)$$

where E_{rec} is the recoil energies in the simulations and a – c are constants obtained in the fitting Eq. (11) to the elstop values (see Fig. 10). The E_{elstop} values were then used in Eq. (2).

To check if this correction was done properly for the DD-BN potential, the mixing was calculated using R^2 -values from simulations which included the stopping and from those without the stopping, but with corrected energies for the AMS and MEA-BN potentials. The resulting values are also included in Fig. 4 and Eq. (12) seems to capture the real effects of the stopping reasonably. The uncertainties in the calculations of the mixing parameters were about $\pm 0.2 \text{ eV/\AA}^5$.

References

- [1] Q. Hou, M. Hou, L. Bardotti, B. Prével, P. Mélinon, A. Perez, Phys. Rev. B 62 (2000) 2825.
- [2] L. Malerba, J. Nucl. Mater. 351 (2006) 28.
- [3] C. Björkas, K. Nordlund, Nucl. Instr. and Meth. B 259 (2007) 853.
- [4] J.F. Ziegler, J.P. Biersack, U. Littmark, The Stopping and Range of Ions in Matter, Pergamon, New York, 1985.
- [5] C.P. Flynn, R.S. Averback, Phys. Rev. B 38 (1988) 7118.
- [6] I. Koponen, Phys. Rev. B 47 (1993) 14011.
- [7] K. Eder, D. Semrad, P. Bauer, R. Golser, P. Maier-Komor, F. Aumayr, M. Peñalba, A. Arnau, J. Ugalde, P. Echenique, Phys. Rev. Lett. 79 (1997) 4112.
- [8] J. Je Page, D.R. Mason, C.P. Race, W.M.C. Foulkes, New J. Phys. 11 (2009) 013004.
- [9] S.-J. Kim, M.-A. Nicolet, R.S. Averback, D. Peak, Phys. Rev. B 37 (1988) 38.
- [10] J. Böttiger, S. Nielsen, H. Whitlow, P. Wried, Nucl. Instr. and Meth. 218 (1983) 684.
- [11] B.M. Paine, R.S. Averback, Nucl. Instr. and Meth. B 7/8 (1985) 666.
- [12] M.W. Finnis, P. Agnew, A.J.E. Foreman, Phys. Rev. B 44 (1991) 44.
- [13] M.P. Allen, D.J. Tildesley, Computer Simulation of Liquids, Oxford University Press, Oxford, England, 1989.
- [14] D.J. Bacon, A.F. Calder, F. Gao, Rad. Eff. Def. Sol. 141 (1997) 283.
- [15] W.G. Kapinos, D.J. Bacon, Phys. Rev. B 53 (1996) 8287.
- [16] D.M. Duffy, A.M. Rutherford, J. Phys.: Condens. Matter 19 (2007) 016207.
- [17] M. Spaczér, A. Almazouzi, R. Schäublin, M. Victoria, Rad. Eff. Def. Sol. 141 (1997) 349.
- [18] A.J.E. Foreman, W.J. Phythian, C.A. English, Rad. Eff. Def. Sol. 129 (1994) 25.
- [19] A. Caro, M. Victoria, Phys. Rev. A (Gen. Phys.) 40 (1989) 2287.

- [20] F. Gao, D. Bacon, T.L.P.E.J. Flewitt, *Model. Simul. Mater. Sci. Eng.* 6 (1998) 543.
- [21] A. Rutherford, D. Duffy, *J. Phys.: Condens. Matter* 19 (2007) 496201.
- [22] G.J. Ackland, M.I. Mendeleev, D.J. Srolovitz, S. Han, A.V. Barashev, *J. Phys.: Condens. Matter* 16 (2004) S2629.
- [23] S.L. Dudarev, P.M. Derlet, *J. Phys.: Condens. Matter* 17 (2005) 1.
- [24] M. Müller, P. Erhart, K. Albe, *J. Phys.: Condens. Matter* 19 (2007) 326220.
- [25] K. Nordlund, L. Wei, Y. Zhong, R.S. Averback, *Phys. Rev. B (Rapid Comm.)* 57 (1998) 13965.
- [26] C. Kittel, *Introduction to Solid State Physics*, third ed., John Wiley & Sons, New York, 1968.
- [27] N.W. Ashcroft, N.D. Mermin, *Solid State Physics*, Saunders College, Philadelphia, 1976.
- [28] P. Ehrhart, *Properties and Interactions of Atomic Defects in Metals and Alloys*, in: *Landolt-Börnstein, New Series III*, Vol. 25, 1991, p. 88 (Chapter 2).
- [29] K. Nordlund, M. Ghaly, R.S. Averback, *J. Appl. Phys.* 83 (1998) 1238.
- [30] D. Terentyev, C. Lagerstedt, P. Olsson, K. Nordlund, J. Wallenius, L. Malerba, *J. Nucl. Mater.* 351 (2006) 65.
- [31] J.F. Ziegler, SRIM-2003 software package, available online <<http://www.srim.org>>.